

## Article

# Effect of Drying Control Agent on Physicochemical and Thermal Properties of Silica Aerogel Derived via Ambient Pressure Drying Process

Natalia Pawlik <sup>1</sup>, Barbara Szpikowska-Sroka <sup>1,\*</sup>, Artur Miros <sup>2</sup>, Bronisław Psiuk <sup>3,4</sup> and Agnieszka Ślosarczyk <sup>5</sup>

<sup>1</sup> Institute of Chemistry, University of Silesia, 9 Szkolna Street, 40-007 Katowice, Poland; natalia.pawlik@us.edu.pl

<sup>2</sup> Łukasiewicz Research Network—Warsaw Institute of Technology, Center for Sustainable Management of Raw Materials and Products, 193A Al. Korfantego Street, 40-157 Katowice, Poland; artur.miros@wit.lukasiewicz.gov.pl

<sup>3</sup> Łukasiewicz Research Network—Institute of Ceramics and Building Materials, Refractory Materials Division, 99 Toszecka Street, 44-100 Gliwice, Poland; psiuk.bronislaw@gmail.com

<sup>4</sup> The “Edith Stein School with Character” Foundation, Bałtycka 8, 44-100 Gliwice, Poland

<sup>5</sup> Institute of Building Engineering, Faculty of Civil and Transport Engineering, Poznan University of Technology, Piotrowo 3, 60-965 Poznan, Poland; agnieszka.slosarczyk@put.poznan.pl

\* Correspondence: barbara.szpikowska-sroka@us.edu.pl

**Abstract:** This paper presents the effect of drying control agents on the physicochemical and thermal properties of hydrophobic silica aerogels derived via the ambient pressure drying (APD) method by a surface silylation using a TMCS/n-hexane mixture. The structural and physicochemical properties of synthesized DMF-modified and unmodified hydrophobic silica aerogels were characterized using Brunauer–Emmett–Teller (BET) analysis, thermo-gravimetric analysis, FT-IR, and Raman spectroscopic techniques. Based on the obtained results, the differences in structure between samples before and after a surface silylation and the effect of drying control agents were documented. The structural measurements confirmed the efficient silylation process (TMCS/n-hexane), as well as the presence of DMF residues of hydrogen bonded with unreacted Si-OH silanol groups within the silica backbone after surface modification. Based on TG analysis, it was found that DMF addition improves thermal resistance (up to 320 °C) and hydrophobic character of prepared aerogel. Modification of the silica aerogel synthesis process by DMF also resulted in a significant increase in BET—the specific surface area, for the unmodified aerogel was ~828 m<sup>2</sup>/g, and for the DMF-modified aerogel more than 1200 m<sup>2</sup>/g—much higher than the value of silica aerogels available on the market.

**Keywords:** silica aerogels; sol-gel method; drying control agents; N,N-dimethylformamide (DMF); silylation; ambient pressure drying



**Citation:** Pawlik, N.; Szpikowska-Sroka, B.; Miros, A.; Psiuk, B.; Ślosarczyk, A. Effect of Drying Control Agent on Physicochemical and Thermal Properties of Silica Aerogel Derived via Ambient Pressure Drying Process. *Energies* **2023**, *16*, 6244. <https://doi.org/10.3390/en16176244>

Academic Editors: Helena M. R. Gonçalves and Marita A. Cardoso

Received: 3 August 2023

Revised: 25 August 2023

Accepted: 26 August 2023

Published: 28 August 2023



**Copyright:** © 2023 by the authors. Licensee MDPI, Basel, Switzerland. This article is an open access article distributed under the terms and conditions of the Creative Commons Attribution (CC BY) license (<https://creativecommons.org/licenses/by/4.0/>).

## 1. Introduction

Silica aerogels are a unique class of highly porous materials (80–99.8%) with large specific surface area (500–1200 m<sup>2</sup>·g<sup>-1</sup>), low thermal conductivity (0.004–0.03 W·m<sup>-1</sup>·K<sup>-1</sup>), low density (0.003–0.5 g·cm<sup>-3</sup>), low refraction index (~1.05), and low dielectric constant (1.0–2.0) [1–6]. Due to their remarkable properties, silica aerogels have become an object of widespread interest in many branches of industry over the past few years, with particular interest in acoustic barriers [7], adsorbents (for oil and organic liquids) [8], sensors [9], catalyst supports [10], and drug delivery systems [11] or aeronautic and astronautic applications [12,13]. Moreover, silica aerogels (even thin layers) are excellent insulating materials compared to traditional insulations, e.g., mineral wool. The super-insulating properties of silica aerogel are due to the air trapped inside the pores within the silica backbone, and the use of silica aerogel-based insulation in the construction industry makes it possible to significantly reduce the thermal conductivity coefficient of

building envelopes and significantly reduce the energy required to maintain buildings. This is extremely important since the construction sector is responsible for nearly 40% of energy consumption, and new innovative insulation materials appear to be one of the key directions to counteract these adverse effects [14–21].

The synthesis of silica aerogels consists of three significant steps, including the sol-gel reaction (1°), gel aging (2°), and drying (3°); the most crucial is the last step because drying type as well as its efficiency determine the final structural and physical properties of fabricated materials. Generally, there are three approaches to the drying step to synthesize aerogels: supercritical drying (SCD), freeze-drying, and ambient pressure drying (APD). The SCD method, usually performed with supercritical carbon dioxide, prevents the pores from collapsing and receiving high-quality aerogels [5,22–24]. Nevertheless, the considerable disadvantages of this drying process include high-cost processing and huge labor risk, which significantly limits the large-scale production of aerogels and their exploitation in commercial applications. Moreover, SCD aerogels are hydrophilic due to the presence of –OH groups on the silica surface, and therefore the structure can collapse and transform into xerogels even in a moderately humid atmosphere [5,23,25–28]. The freeze-drying pathway may damage the porous structure, which results in obtaining macroporous materials [5]. To overcome these inconveniences, an alternative and more practical APD method via solvent-exchange step using low surface tension solvents, LSTS, and silylating agents is implemented [5,24].

Among various organic compounds, hexamethyldisiloxane (HMDSO) and trimethylchlorosilane (TMCS) are frequently used for silylation. Such a process involves a replacement of the –H hydrogen atom from the hydrophilic Si–OH silanol group on hydrophobic –SiR<sub>3</sub> (e.g., Si(CH<sub>3</sub>)<sub>3</sub>) trialkylsilyl one, which successfully prevents the structure collapse provoked by capillary forces and deterioration in a humid environment [29,30]. Due to the above arguments, a significant interest in aerogels synthesis via APD method was observed in recent years, which could be confirmed by a growing number of publications in this field [26,30–36].

The structure of silica aerogels can be successfully controlled by introducing some organic solvents during the preparation process, commonly known as drying control chemical additives, DCCAs [37]. Among the drying control chemical additives that have so far been used in modifying the structure of silica aerogels, the most common were formamide (FA), N-methyl formamide (NMF), N-N-dimethyl formamide (DMF), acetamide (AA), glycerol (GLY), and oxalic acid (OXA). There have also been recent publications in which oxalic acid and glycerol were used as a modifier for aerogels synthesized from water glass and methyltrimethoxysilane (MTMS), respectively [38–40].

A study by Parvathy Rao et al. showed that the type of DCCAs used significantly affects the gelation rate, density, and shrinkage during drying of silica aerogels made from TEOS; for example, the gelation time shortened in the following order: FA > NMF > AA > GLY > OXA > DMF, while volume shrinkage was about 20% lower for DCCAs modified aerogels than for unmodified ones, and decreased in the order: OXA > GLY > DMF > AA > NMF > FA, which was associated with an increase in pore size in the same order: OXA > GLY > DMF > AA > NMF > FA. The above parameters significantly affected the final bulk density of aerogels, which decreased in order: FA > NMF > AA > DMF > GLY > OXA [38]. By analyzing the results of the study by Parvathy Rao et al., it can be seen that DMF, as aprotic DCCAs, promotes the development of a porous structure of aerogels, which translates into a relatively low aerogel density and, at the same time, allows a shorter gelation time. These parameters favor the excellent properties of silica aerogels, i.e., a high specific surface area, which is a decisive factor for the insulating properties of this material and the broader use of silica aerogel as an insulating material in construction. There are currently two trends in the construction industry, the first leading to the synthesis of hydrophobic mats and the second to the use of aerogel granules, either as an insulating layer for glazing or as a filler in paints, plasters, or mortars and concretes. The latter is currently under development, and many research centers are investigating

these materials as potential solutions for construction. Nevertheless, they generally use commercially available silica aerogel granules with average specific surface areas between 600 and 900 m<sup>2</sup>/g as granules [41–46].

In contrast to commercial products, in the study presented here, we introduced aprotic DMF as a modification of the gelation stage. In the second stage, we applied silylation with TMCS to obtain a granulate with the highest possible specific surface area. Both processes counteract the collapse of the silica aerogel structure, leading to a more durable and hydrophobic structure.

The influence of DMF on aerogels' structure, and thus on their properties, is described below. Due to DMF molecules' relatively strong dipole moment, they can interact with H<sub>2</sub>O and Si-OH (e.g., from hydrolyzed TEOS) via hydrogen bonds. Since the polarity of the O-H bond in H<sub>2</sub>O is stronger than in the silanol Si-OH group, DMF mainly combines with H<sub>2</sub>O and slightly with Si-OH. Such interactions can only be observed if the addition of DMF into the reaction system is relatively small. On the other hand, if the amount of introduced DMF agent is greater, the increasing part of DMF molecules can also attach -OH moieties from a hydrolyzed precursor. As a result, a part of the hydrogen-bonded Si-OH groups is efficiently blocked during the condensation reaction, and finally, the gelation step is elongated compared to native silica aerogels. As was reported in the available literature, the hydrogen bond between DMF and -OH groups could be destroyed during the high-temperature silylation and drying step in the APD procedure. Then, the previously hydrogen-bonded -OH groups condense, and consequently, the porous structure collapses [30,47].

Generally, the synthesis of DMF-modified silica aerogels from water glass, tetraethoxysilane (TEOS), and 'methyl silicate 51' via APD [30,47–49] and SCD [37,50,51] methods have been presented in the literature. Nevertheless, there is still a gap in the interpretation of the effect of DMF on the physicochemical properties of silica aerogels, including the lack of description of aerogels synthesis where DMF molecules are still present in silica porous structure after an efficient surface modification process. These observations became the motivation for investigating silica aerogels modified with drying control agents presented in this article. Therefore, in the present paper the structural and physical properties of DMF-modified silica aerogel obtained via the ambient pressure drying method (APD) using a TMCS/n-hexane silylation solution were outlined. The influence of drying control agent additive through hydrogen bonding with silica backbone on the final aerogel's properties was discussed in detail. Determined parameters: BET specific surface area (SBET), average pore diameter, total pore volume per unit mass, density, and thermal stability of fabricated silica aerogels were considered in the context of DMF chemical modification. Moreover, the changes in functional groups were identified using scanning electron microscopy and Fourier-transformed infrared (FT-IR) and Raman spectroscopic techniques.

## 2. Materials and Methods

### 2.1. Chemicals and Reagents

All reagents used in the preparation were of analytical grade and used without further purification. The precursor used for the preparation of alcogels, tetraethoxysilane (TEOS), was supplied by Sigma-Aldrich (St. Louis, MI, USA), similar to N,N-dimethylformamide (DMF) used as a chemical modifier. Ethyl alcohol (EtOH), ammonium hydroxide 25%, and hydrochloric acid 35–38% were purchased from POCH Co, Gliwice, Poland. The silylation process was performed by a mixture of trimethylchlorosilane (TMCS) (from Sigma-Aldrich) and n-hexane (from POCH Co.). Prepared aerogel samples without DMF addition and with DMF modifier were denoted as AG1 and AG2, respectively.

### 2.2. Samples Preparation Procedure

The procedure of silica aerogels synthesis involved three stages: synthesis of silica alcogels by a two-step acid-base catalysis (1), surface modification using TMCS/n-hexane

solution (2), and drying of wet gel at room temperature (3). Each stage was carried out as follows:

- (1) A mixture of TEOS in ethyl alcohol was prepared, and an appropriate amount of hydrochloric acid (at a concentration of 0.1 mol/L) was added to achieve  $\text{pH} \approx 2$ . In the case of AG2 sample, DMF was introduced simultaneously with TEOS and ethanol. The obtained mixtures were sealed and vigorously stirred for 30 min. Next, the ammonium hydroxide solution (0.5 mol/L) was added dropwise into initial mixtures to adjust  $\text{pH} \approx 6$  and stirred for a few minutes until gelation occurred. The volume ratios of the components used during samples preparation equaled:  $\text{TEOS}:\text{EtOH} = 1:1$  (AG1) and  $\text{TEOS}:\text{EtOH}:\text{DMF} = 1:1:0.5$  (AG2).
- (2) Obtained silica gels were aged in ethyl alcohol for seven days to strengthen the gel network and exchange the pore fluids with a volatile liquid.
- (3) Obtained silica alcogels were treated with a mixture of TMCS and n-hexane (1:5 volume ratio) at  $50^\circ\text{C}$  for two days for surface modification. After the silylation process, the prepared samples were dried under ambient pressure to remove all liquids from the porous structure.

The synthesis pathway of studied silica aerogels is presented in Figure 1. Moreover, the analogous silica xerogels were prepared via (1) synthesis step and dried without TMCS/n-hexane surface modification. Xerogel samples were denoted as XG1 and XG2, respectively, and their structural properties were compared with AG1 and AG2 aerogels.

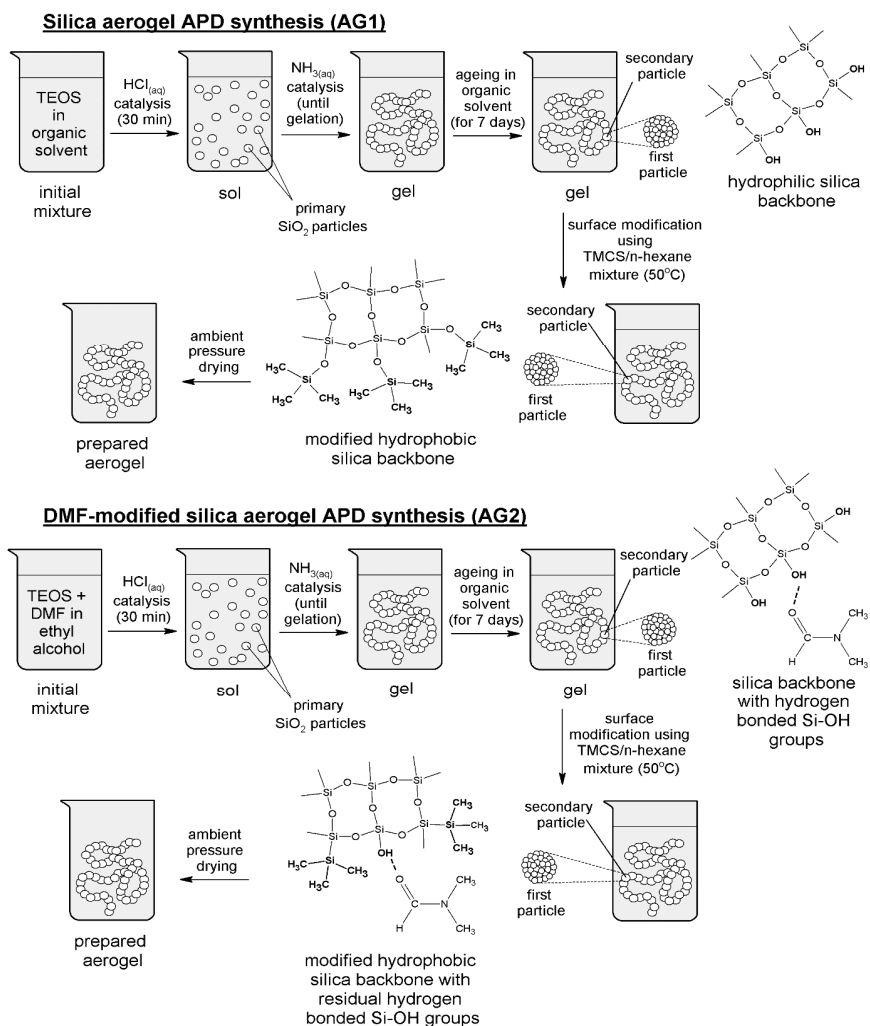


**Figure 1.** The scheme demonstrated an applied preparation procedure of AG1 and AG2 silica aerogels via ambient pressure drying.

### 2.3. Material Characterization

The structural and physical characterization of synthesized aerogels was performed using adsorption isotherms and thermo-gravimetric analysis, scanning electron microscopy (SEM), FT-IR, and Raman spectroscopic techniques. The surface area and pore volume of silica aerogel materials were estimated based on adsorption isotherms in low-temperature nitrogen sorption at 77 K (ASAP 2010, Micrometrics, Ottawa, ON, Canada). The average diameters of the pores were calculated based on nitrogen adsorption isotherms with the BET method, based on the  $4V/\bar{A}$  formula, where  $V$  stands for total pore volume determined in a single point of adsorption isotherm with  $p/p_0 = 0,99$ . The specific surface areas were calculated using the Brunauer–Emmett–Teller (BET) equation. Thermo-gravimetric analysis of aerogels was performed in an argon atmosphere using NETSCH apparatus, type TG 209 F3. During measurements, the following parameters were used: flow rate of inert gas (Ar) 150 mL/min, speed of sample heating  $10\text{ }^\circ\text{C}/\text{min}$ , and temperature range  $30\text{--}1000\text{ }^\circ\text{C}$ . Micrographs of the investigated samples surfaces were taken using a high-resolution scanning electron microscope Mira 3 (Tescan). The FT-IR spectra were registered on the Nicolet iS50 ATR spectrometer in  $500\text{--}4000\text{ cm}^{-1}$  frequency region to identify the functional groups on the surface. The Raman scattering was excited by DXRxi Raman Imaging Microscope using the 532 nm laser line with an output power of 10 mW in  $250\text{--}3250\text{ cm}^{-1}$  spectral range. The experiments were performed with a confocal 50x objective.

### 3. Results and Discussion

The FT-IR and Raman spectroscopic techniques were used to investigate the presence of appropriate functional groups and chemical linkages formed within silica structures. The FT-IR spectra registered for prepared xerogels: XG1 and XG2 were presented in Figure 2.

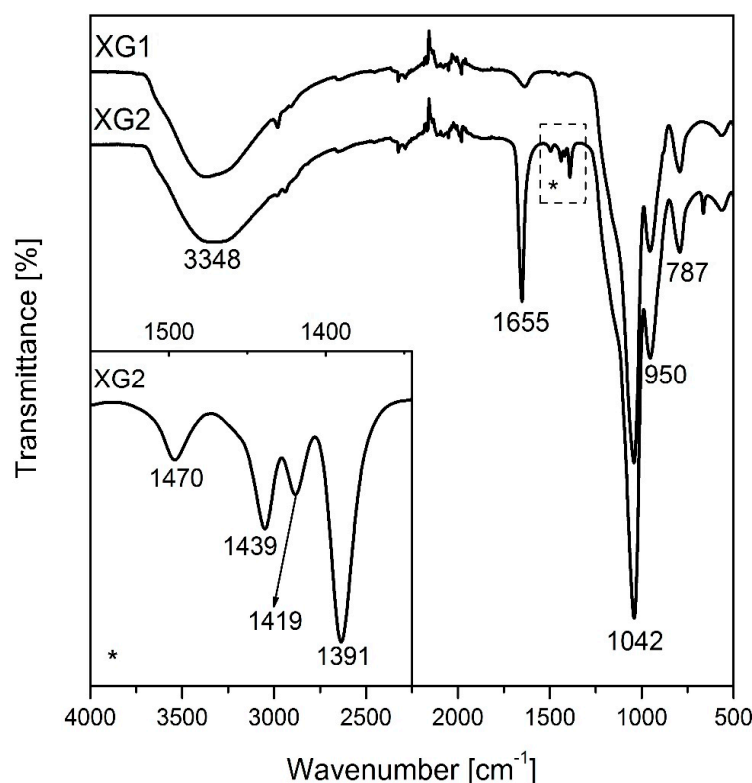


**Figure 2.** FT-IR spectra registered for silica xerogels obtained via ambient pressure drying without TMCS/n-hexane surface modification. Inset, marked as \*, shows  $1345\text{--}1550\text{ cm}^{-1}$  region for DMF-modified xerogel sample (XG2).

All IR bands (also for aerogels, see in Figure 3) were assigned based on literature data [52–58]. Registered FT-IR spectra reveal weak bands at  $\sim 2980\text{ cm}^{-1}$  and  $\sim 2931\text{ cm}^{-1}$ , corresponding to symmetric (vs) and asymmetric (vas) C-H vibrations derived from ethanol residues. Moreover, other IR bands registered for XG1 and XG2 samples were easily identified as stretching vibrations originating from the silica backbone. The strongest peak near  $\sim 1042\text{ cm}^{-1}$  was assigned to asymmetric vibrations (vas) within Si-O-Si siloxane bridges. Other bands, which are located at the following frequency regions:  $\sim 950\text{ cm}^{-1}$ ,  $\sim 787\text{ cm}^{-1}$ , and  $\sim 550\text{ cm}^{-1}$ , were assigned to: Si-O vibrations, Si-O-Si stretching, and bending vibrations ( $\delta$ ) from O-Si-O groups, respectively. The IR spectrum registered for XG2 xerogel sample reveals some bands, which confirm the presence of DMF molecules within a sol-gel structure. A relatively intense IR band located at  $\sim 1655\text{ cm}^{-1}$  is related to C=O stretching in formyl groups, but it may also be derived from Si-OH vibrations. Moreover, the following peaks:  $1391\text{ cm}^{-1}$ ,  $1419\text{ cm}^{-1}$ ,  $1439\text{ cm}^{-1}$ , and  $1470\text{ cm}^{-1}$  could be assigned to different types of C-H vibrations within DMF molecules. It should be noticed that the IR band corresponding to  $\text{H}_3\text{C-N}$  stretching from DMF ( $\sim 2775\text{ cm}^{-1}$ ) is covered by a wide O-H band located between  $\sim 2690\text{ cm}^{-1}$  and  $\sim 3710\text{ cm}^{-1}$  frequency region.

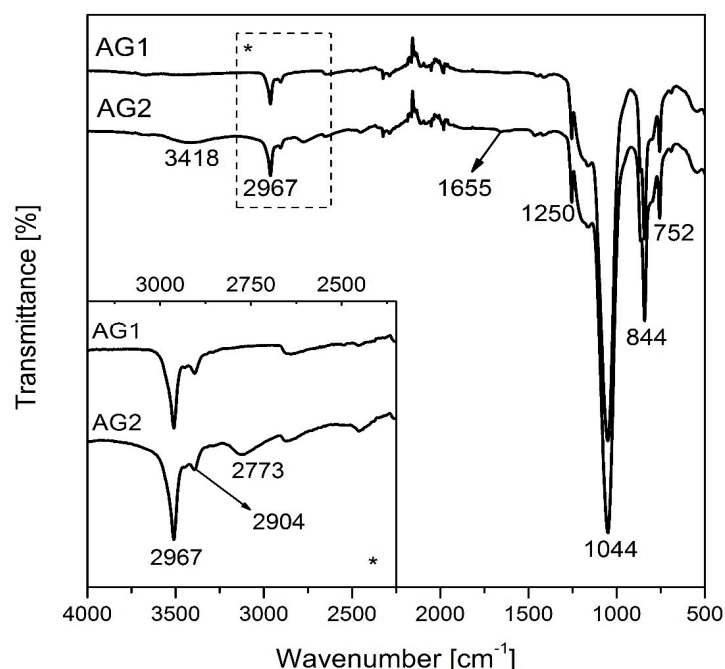


**Figure 3.** FT-IR spectra registered for fabricated silica aerogels. Inset, marked as \*, shows an enlargement of the spectra in the  $2350\text{--}3200\text{ cm}^{-1}$  frequency region in order to reveal the spectral differences.

An intense IR band originated from O-H stretching vibrations within Si-OH silanol groups with a maximum of  $\sim 3350\text{ cm}^{-1}$  was detected for both xerogel samples. The free silanol groups on the XG1 sample's surface undergo a condensation reaction, and in consequence, neighboring Si-OH groups create new Si-O-Si linkages. The described effect leads to structure collapse. In the case of DMF-modified xerogel XG2, the hydrogen bond with Si-OH groups can be created, and therefore, Si-OH groups are partially blocked from the condensation reaction, and the structure is collapsed. Moreover, numerous silanol Si-OH groups in both prepared xerogels are responsible for the hydrophilic nature of resulting structures. Due to the above arguments, further surface modification with TMCS/n-hexane is justified; therefore, a hydrophobization process was performed during aerogels preparation.

Figure 3 presents the FT-IR spectra measured for prepared silica aerogel samples after the silylation process.

The registered IR spectra display a few bands within 2350–3250  $\text{cm}^{-1}$  and 500–1300  $\text{cm}^{-1}$  frequency regions, specific to C-H and silicate network vibrations, respectively. The peaks at  $\sim 2967 \text{ cm}^{-1}$  and  $\sim 2904 \text{ cm}^{-1}$  were registered for both prepared samples, which could be assigned to symmetric (vs) and asymmetric stretching (vas) modes of C-H in  $-\text{CH}_3$  groups. Furthermore, the weak peak near  $\sim 1410 \text{ cm}^{-1}$  spectral range corresponds to asymmetric deformation vibrations ( $\delta_{\text{as}}$ ) within the C-H moiety. The presence of such bands in FT-IR spectra confirms the effective surface modification via conducted silylation process.

In the 500–1300  $\text{cm}^{-1}$  region, a signal that appears at  $\sim 1250 \text{ cm}^{-1}$  as a shoulder could be assigned to deformation vibrations of Si-CH<sub>3</sub> groups. The presence of this IR band confirms the successful attachment of non-polar  $-\text{Si}(\text{CH}_3)_3$  groups from TMCS molecules, and then, the silica surface becomes hydrophobic. Other IR signals which are related to the hydrophobic nature of studied aerogels (induced by Si-C vibrations) are located at  $\sim 840 \text{ cm}^{-1}$  and  $\sim 752 \text{ cm}^{-1}$ . The registered spectra also exhibit some bands originating from the silica network:  $\sim 1044 \text{ cm}^{-1}$  (asymmetric vibrations (vas) of Si-O-Si linkages) and  $\sim 550 \text{ cm}^{-1}$  (bending vibrations ( $\delta$ ) from O-Si-O bridges).

The presence of residual DMF molecules within the silica porous structure after the silylation process could be confirmed by the IR peak located at  $\sim 2773 \text{ cm}^{-1}$ , which is related to  $\text{H}_3\text{C-N}$  stretching vibrations. The broadband with the maximum at  $3418 \text{ cm}^{-1}$ , as well as the weak peak at  $1655 \text{ cm}^{-1}$  registered for AG2 aerogel sample, suggest the presence of residual hydrogen-bonded unreacted Si-OH silanol groups, which are still present after the performed silylation process. These results can also be confirmed by thermo-gravimetric analysis.

The Raman spectra were also registered and studied to further investigate the structure of prepared aerogel samples (Figure 4).

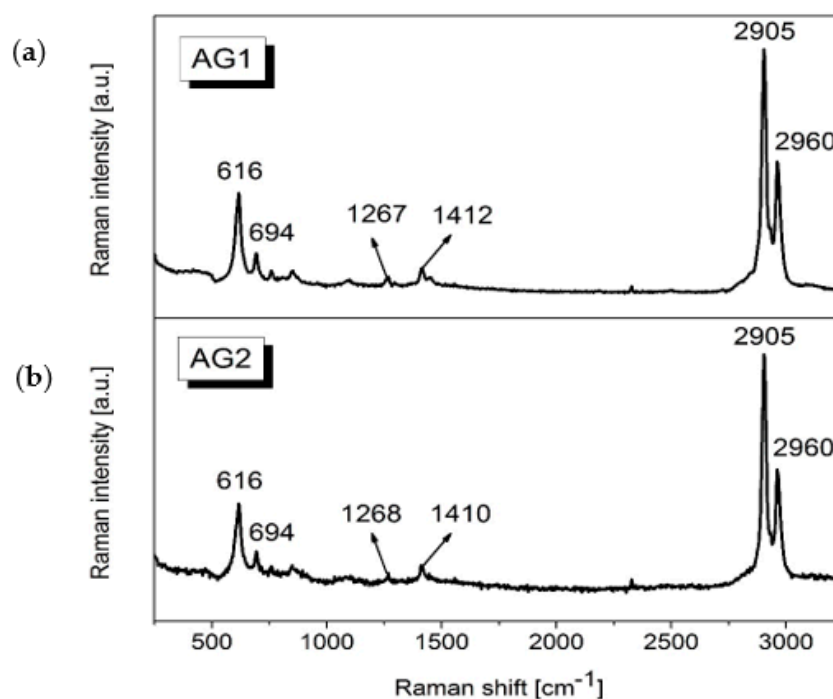


**Figure 4.** Raman spectra registered for prepared silica aerogels: (a) pure silica aerogels AG1 and (b) DMF-modified silica aerogels AG2.

Each Raman spectrum was recorded on a sample surface, and the characteristic Raman peaks appeared from 250  $\text{cm}^{-1}$  to 3250  $\text{cm}^{-1}$ . The registered Raman lines were identified based on literature data [23,59–63]. A band registered for each sample at  $\sim 616 \text{ cm}^{-1}$  is a defect line attributed to Si-O stretching within  $(\text{SiO})_3$ -ring breathing mode. Another Raman band located at  $\sim 694 \text{ cm}^{-1}$  could be interpreted as rocking vibrations from Si-CH<sub>3</sub>,

which confirms that the performed silylation process was efficient. Therefore, obtained materials are hydrophobic. Finally, the Raman signals located at  $\sim 1250\text{ cm}^{-1}$ ,  $\sim 1412\text{ cm}^{-1}$ ,  $\sim 2905\text{ cm}^{-1}$ , and  $\sim 2960\text{ cm}^{-1}$  could be identified as C-H stretching in  $-\text{CH}_3$  groups.

The micrographs presented in Figure 5 show that both investigated aerogel samples are formed by relatively highly packed grains with an isometric shape with diameters below 100 nm.

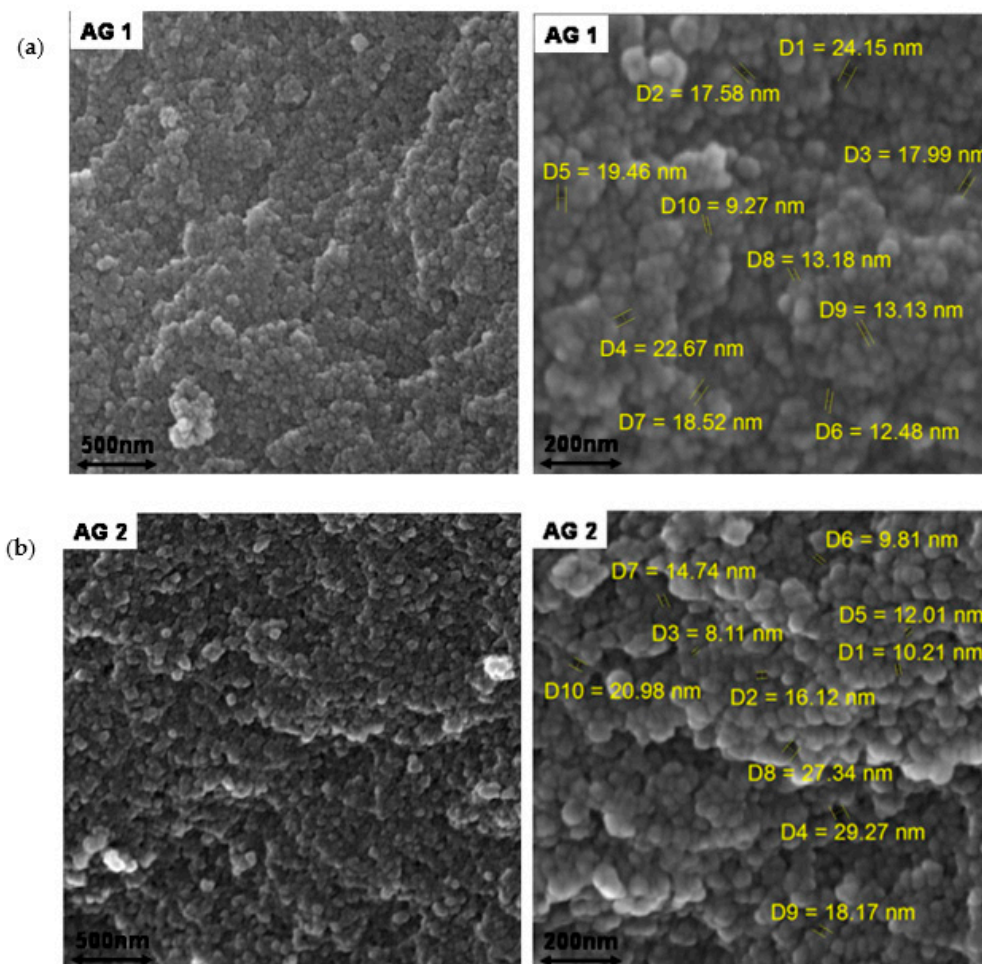


**Figure 5.** SEM micrographs of (a) pure silica aerogels AG1 and (b) DMF-modified silica aerogels AG2. Micrographs taken at 100,000 $\times$  and 250,000 $\times$  (with marked dimensions of selected pores) SEM magnifications.

The finer pores were identified between the grains, and the observed effect is consistent with the well-known fact that the pore diameter is any fraction of the diameter of closely stacked grains of a mono-fraction. The dimensioning of the pores allowed us to conclude that the dominant contribution to the samples' microstructures has pores with diameters from a few to thirty nanometers. However, for the DMF-modified AG2 samples, the observed pore fraction has a noticeably wider range compared with AG1 samples. Moreover, based on the topography of prepared aerogels, the AG2 samples' surface seems more folded. It could also be concluded that high specific surface areas characterize both types of prepared aerogels. However, such a value should be higher for modified AG2 samples. Generally, the microstructure observations from the SEM method are consistent with BET analysis.

Figure 6 shows the adsorption/desorption isotherms obtained for pure unmodified (AG1) and DMF-modified (AG2) aerogels, and simultaneously, the pore size distribution (PSD) was demonstrated in Figure 7.

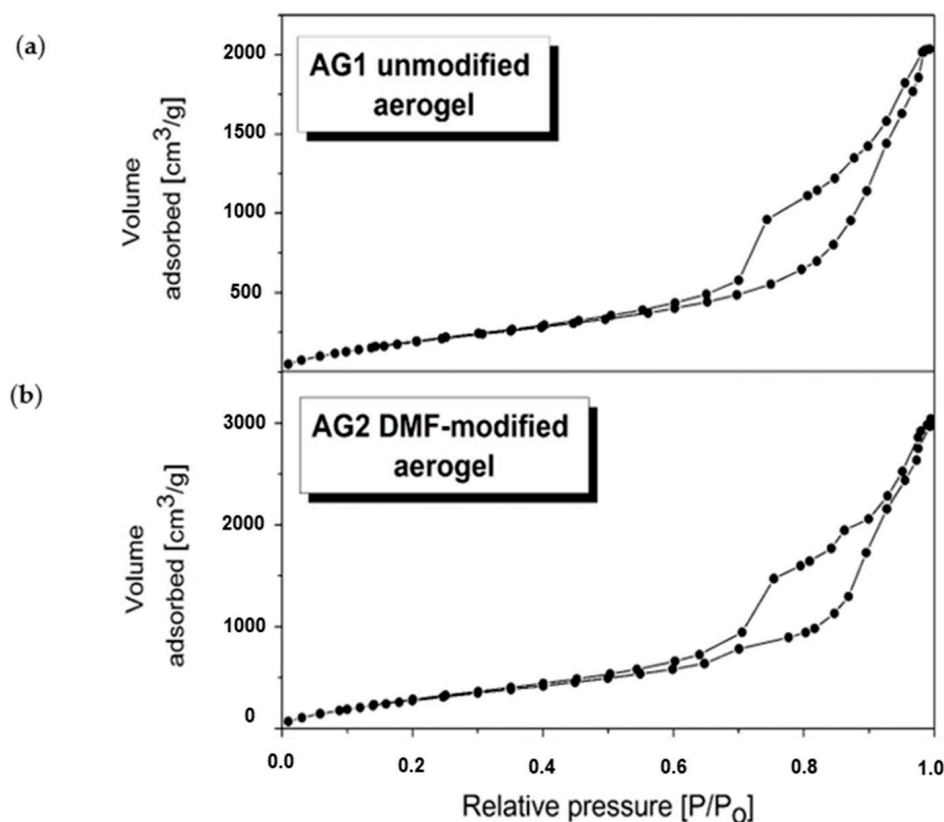


**Figure 6.** Adsorption/desorption isotherms obtained for (a) pure silica aerogels AG1 and (b) DMF-modified silica aerogels AG2.

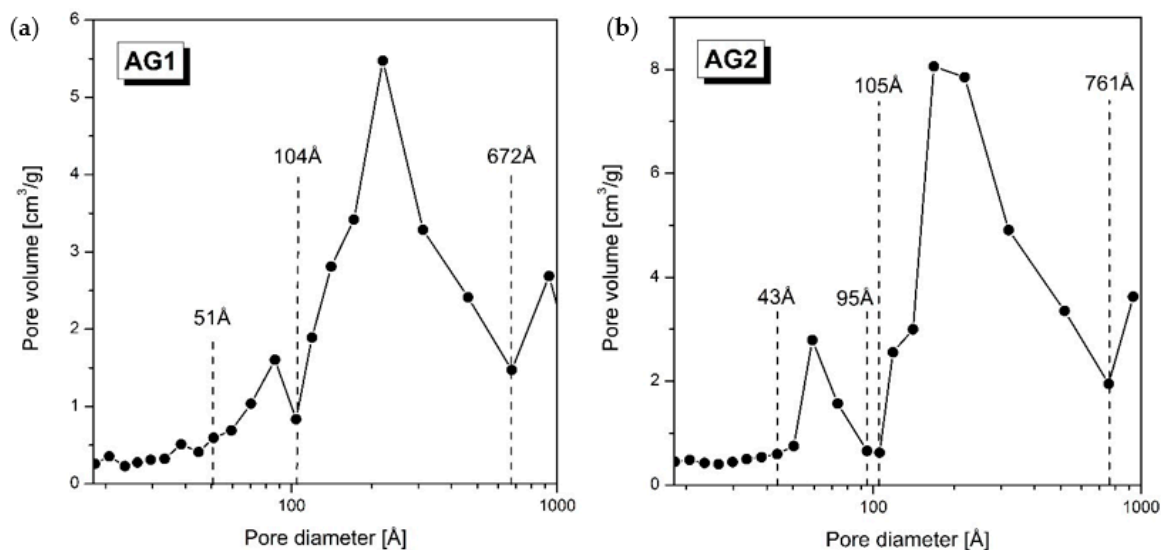


**Figure 7.** PSD of (a) pure silica aerogels AG1 and (b) DMF-modified silica aerogels AG2.

For the prepared aerogels, the shape of adsorption/desorption isotherms corresponds to the mesoporous structure. According to the classification of porous materials made by de Boer in 1958, the shape of the desorption hysteresis loop indicates the pore structure with both cylindrical capillary pores open at both ends and cylindrical pores closed at one end with a narrow neck at the other, like an ink bottle. The average pore diameters for both materials are the same and equal to 13.2 nm. The differences appear only in the shape of curves depicting the PSD. On the PSD curve for pure silica aerogel (AG1), there

are two visible peaks: the main broad peak corresponding to the pores with the diameters between 104 Å and 672 Å and the smaller one, not completely created, corresponding to the pore diameters in 51–104 Å range. For DMF-modified aerogel, the PSD profile is quite similar. The broad peak is observed in a range from 105 Å to 761 Å, and the smaller one in a range from 43 Å to 95 Å. Therefore, as shown in Figure 7, the DMF-modified sample exhibits a slightly broader size distribution. Generally, as was described in the available literature, the uniformity of pore size distribution is strictly related to the amount of introduced DMF additive during the synthesis procedure. If a moderate amount of DMF is added during preparation ( $n_{\text{Si}}:n_{\text{DMF}} > 1$  (molar ratio)), in that case, the PSD should be narrow due to the perforation of condensation reaction in some well-organized way compared to unmodified analogous samples, where condensation is quick and disordered. However, the PSD is wider if DMF excess is introduced during synthesis. This is because the hydrogen bond between Si-OH groups and DMF molecules is usually destroyed after the silylation process [30]. As a result, the big difference in capillary pressure operated on pores made the structure collapse during ambient pressure drying, which leads to broader pores size distribution. In the case of our proposed silylation conditions, the DMF residual molecules are still present within silica pores. Therefore, we suppose that PSD for the AG2 sample is only slightly broader compared to AG1 one (the difference between pore diameter between AG1 and AG2 is about  $\sim 90$  Å). Generally, the PSD distribution of studied aerogels is relatively narrow compared to other APD aerogels described in the literature. He et al. presented the results for DMF-modified and unmodified water glass-based aerogels in a range from 17 Å to 17000 Å [30] and from 17 Å to 500 Å [47]. In the case of DMF-modified samples presented in work [30], if  $n_{\text{Si}}:n_{\text{DMF}}$  molar ratio was equal to 2.23, the PSD peak was narrower compared to the unmodified sample. Successively, if  $n_{\text{Si}}:n_{\text{DMF}}$  decreased to 1.11 and 0.83, the PSD peaks were broader than those of the unmodified aerogel. The difference in the widths of the peaks reached up to 700 Å. A similar effect was also reported for DMF-modified silica samples described in the work [47]. When the  $n_{\text{Si}}:n_{\text{DMF}}$  molar ratio was higher than 1, the PSD peaks were narrower than unmodified ones. However, if  $n_{\text{Si}}:n_{\text{DMF}}$  was lower than 1, the PSD distribution was broader, and the final PSD differences between DMF-modified and unmodified samples were about  $\sim 300$ – $400$  Å. In the case of our prepared samples, the difference in PSD peaks width was only  $\sim 90$  Å. This could be explained by residual amounts of DMF molecules after the silylation process with TMCS/*n*-hexane, despite introducing DMF in excess during the proposed synthesis ( $n_{\text{Si}}:n_{\text{DMF}} = 0.68$ ).

Based on sorption isotherms with Brunauer–Emmett–Teller (BET) analysis, the specific surface areas of prepared silica aerogel samples were also determined. The BET-specific surface area determined for AG1 sample is equal to  $\text{SBET} = 828 \text{ m}^2/\text{g}$ . This value is very similar to surface areas determined for other TEOS-based systems obtained via the APD method:  $\text{SBET} = 878 \text{ m}^2/\text{g}$  [49] and SCD route:  $\text{SBET} = 875 \text{ m}^2/\text{g}$  [37]. As is seen from Table 1, BET surface areas determined for analogous silica water–glass-based aerogels do not reach such high values. The DMF-modified silica aerogel (AG2) exceeds a very high BET surface area equal to  $1231 \text{ m}^2/\text{g}$ .

The BET surface area values higher than  $1000 \text{ m}^2/\text{g}$  were also obtained for only a few aerogels prepared through ambient pressure drying and described by Wu et al. (up to  $1005 \text{ m}^2/\text{g}$ ) [26] and Nazriati et al. (up to  $1113.76 \text{ m}^2/\text{g}$ ) [64]. Such high specific surface areas are rather typical for supercritical drying systems, e.g., as was presented in the following publications [56–58,65]. Based on published data, it was observed that for DMF-modified aerogels with  $n_{\text{Si}}:n_{\text{DMF}}$  molar ratio equal to about 0.65, the increase in surface area values was achieved at about 6.2% [47] and 6.8% [49] levels compared to pure silica samples. In the case of our DMF-modified sample (AG2,  $n_{\text{Si}}:n_{\text{DMF}} = 0.68$ ), the increase in surface area reached up to 48.7% of BET surface area in comparison to TEOS-based aerogel without DMF modification (AG1).

**Table 1.** The literature data of specific surface areas measured for DMF-modified silica aerogels by isotherms with standard Brunauer–Emmett–Teller (BET) analysis.

Silica Source	Used Catalyst(s)	Drying Method	Surface Modification	DMF:Si Molar Ratio	BET Surface Area (m <sup>2</sup> /g)	Ref.
Si(OC <sub>2</sub> H <sub>5</sub> ) <sub>4</sub> (TEOS)	HCl NH <sub>3</sub> ·H <sub>2</sub> O	APD	TMCS in n-hexane	0.50	1231	Present work
Na <sub>2</sub> O:3.33 SiO <sub>2</sub>	HCl	APD	TMCS in n-hexane	0		[30]
				0.30		
				0.45	469	
				0.90	551	
				1.20	680	
Si(OC <sub>2</sub> H <sub>5</sub> ) <sub>4</sub> (TEOS)	C <sub>6</sub> H <sub>8</sub> O <sub>7</sub> ·H <sub>2</sub> O (citric acid)	SCD		0	875	[37]
				0.2	860	
				0.4	830	
				0.6	770	
				0.8	655	
Na <sub>2</sub> O:3.55 SiO <sub>2</sub>	NH <sub>3</sub> ·H <sub>2</sub> O	APD	TMCS in n-hexane	0	740	[47]
				0.31	817	
				0.62	728	
				0.93	627	
				1.24	456	
Si(OC <sub>2</sub> H <sub>5</sub> ) <sub>4</sub> (TEOS)	HCl, NH <sub>3</sub> ·H <sub>2</sub> O	APD	TMCS in isopropyl alcohol (IPA)	1.55	786	[49]
				0	878	
				0.5	939	
				1.0	927	
				1.5	938	
				2.0	939	
				2.5	894	
3.0	930					
	3.5	908				
	4.0	935				

Generally, as could be seen from the PSD in Figure 7, the modification of silica aerogel by DMF additive diminishes the diameters of the pores, which in consequence leads to the higher amount of micropores within the aerogel's structure and gives the higher specific surface area of prepared material (AG2, SBET = 1231 m<sup>2</sup>/g) compared to unmodified aerogel (AG1, SBET = 828 m<sup>2</sup>/g). Moreover, the BET microstructure analysis pointed out that in the case of DMF-modified silica aerogel, the micropore volume is about 30% higher than for pure silica samples and amounts to 4.1 cm<sup>3</sup>/g. The aerogels' structure also affected the density, and for the AG1 sample, it equaled 0.115 g/cm<sup>3</sup>, while for AG2 aerogel, it was negligibly smaller and equaled 0.114 g/cm<sup>3</sup>. To summarize, the selected structural and thermal properties of studied samples are collated in Table 2.

**Table 2.** Structural and thermal parameters of pure silica aerogel (AG1) and modified with DMF (AG2).

	Density (g/cm <sup>3</sup> )	Surface Area (m <sup>2</sup> /g)	Average Pores Diameter (nm)	Micropores Volume (cm <sup>3</sup> /g)	Mass Changes at 2% Mass Loss	Temperature 4% Mass Loss	(°C): 10% Mass Loss
AG1	0.115	828	13.2	2.7	90	390	800
AG2	0.114	1231	13.2	4.1	310	350	630

In Figure 8, the thermogravimetric (TG) curves for pure AG1 and DMF-modified AG2 silica aerogels are presented. The thermal stability of prepared aerogels was evaluated in a temperature range from 30 °C up to 1000 °C. Generally, two main stages of weight loss for both of prepared aerogels were registered: the first stage was detected as gentle degradation. However, the second one was observed as a major continuous weight loss. For the AG1 sample, the following degradation steps were detected: ~30–162 °C (1°) and ~273–1000 °C (2°), while the range from 162 to 273 °C was registered without weight loss. In the case of the AG2 DMF-modified sample, the degradation steps were observed in the following temperature ranges: ~30–49 °C (1°) and ~199–1000 °C (2°), while the range between 49 and 199 °C was registered without weight loss. The total weight losses were estimated at 11.25% and 15.97% for AG1 and AG2 samples, respectively. Generally, the first weight-loss step for both prepared aerogels is attributable to removing adsorbed water.

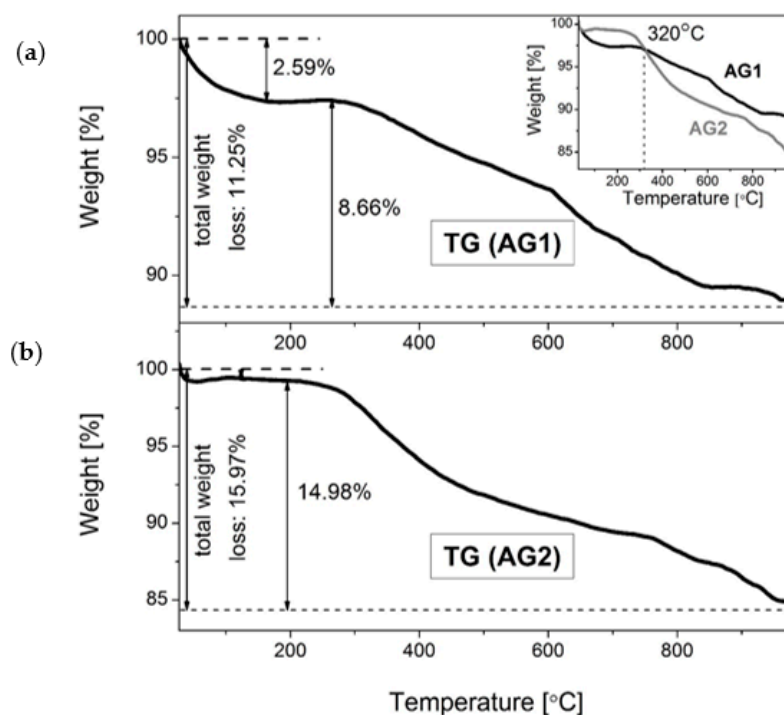
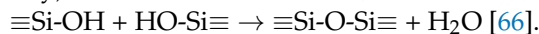


**Figure 8.** TG curves obtained for (a) pure silica aerogels AG1 and (b) DMF-modified silica aerogels AG2. Inset shows the comparison of thermal resistance of prepared aerogels in the range from 30 to 1000 °C.

The presented results suggest that the amount of unmodified silanol Si-OH surface groups that interact with water molecules is slightly higher for AG1 aerogel than AG2. This is evidenced by a more significant weight loss for the AG1 sample during the first step of thermal degradation (for AG1: 2.59% and for AG2: 0.99%). On the other hand, the total amount of Si-OH groups within the silica backbone is greater for AG2 DMF-modified aerogel (as evidenced by an infrared band with a maximum at  $\sim 3420\text{ cm}^{-1}$ , see Figure 3) due to a hydrogen bonding with DMF molecules. Consequently, for the DMF-modified sample (AG2), the amount of non-hydrogen-bonded Si-OH groups is smaller. Therefore, the AG2 aerogel seems to be more hydrophobic than the unmodified AG1 one (despite the broad IR band near  $\sim 3420\text{ cm}^{-1}$ ), and the final weight loss during the first TG step is smaller for the DMF-modified sample due to the smaller amount of bonded water. Consequently, it could be concluded that the AG2 sample reveals better temperature resistance at lower temperatures. The next weight loss step is more spectacular for both prepared samples and was estimated to be 8.66% for AG1 and 14.98% for AG2. The second degradation step is closely related to the thermal evolution of the organic part of studied aerogels. It should be noted that the second-step weight loss starts at  $\sim 160\text{ °C}$  for the DMF-modified

aerogel (AG2) due to the gradual evaporation of DMF additive from silica backbone (boiling point of DMF: ~153 °C [48]). Then, the non-hydrogen bonded Si-OH groups (which were not reacted during the condensation reaction at the beginning of the presented synthesis pathway) can react with each other, which leads to densify of silica:



The weight loss for AG1 non-modified silica sample starts at a higher temperature (~200 °C) due to the lack of DMF molecules within the silica network. Therefore, such an effect could explain the more significant weight loss for the AG2 aerogel sample and better temperature resistance for AG1 at higher temperatures. The significant continuous weight loss started from ~270 °C for both prepared samples. This effect is strictly related to the thermal decomposition of Si-(CH<sub>3</sub>)<sub>3</sub> modified groups, which are mainly responsible for the hydrophobic nature of studied aerogels [67]. Obtained thermogravimetric results are in good agreement with FT-IR studies.

#### 4. Conclusions

The presented research studied the influence of drying control agent modification on the physical and chemical properties of silica aerogel synthesized by ambient pressure drying. Particular attention was focused on the role of DMF in creating the microstructure of silica aerogel. Scanning electron microscopy (SEM) studies indicated highly paced microstructures of prepared aerogels. The FT-IR and Raman measurements confirmed the presence of DMF molecules within the silica aerogel skeleton, even after the subsequent treatment in TMCS/n-hexane solution. The DMF modification led to the microstructure with higher amounts of micropores with broader size distribution and a very high surface area equal to about 1231 g/cm<sup>3</sup>. Such a high surface area was comparable with the values obtained by other researchers for silica aerogels dried in supercritical conditions (SCD) and significantly higher than the surface areas obtained via ambient pressure drying (APD).

Furthermore, the addition of DMF followed by the silylation process in APD influenced excellent structural parameters and thermal stability of received silica aerogel and promoted its hydrophobic nature. The TG analysis revealed that prepared aerogels retained the stable structure up to ~270 °C due to Si-(CH<sub>3</sub>)<sub>3</sub> modified groups.

The resulting silica aerogel, due to the simultaneous modification with DMF and TMCS, has a much higher specific surface area than most commercial silica aerogels and could be an interesting material for use in granular form in paints, plasters, or mortars and concretes. In particular, the use of silica aerogels in lightweight and ultralight cementitious composites appears to be important due to the significant improvement in insulation performance. This is an important trend in the construction industry, in line with the sector's drive for sustainability.

**Author Contributions:** Conceptualization, B.S.-S. and A.M.; methodology, B.S.-S. and N.P.; software, B.S.-S.; validation, B.S.-S., N.P., A.M. and A.Š.; formal analysis, B.S.-S., N.P., A.M. and A.Š.; investigation, B.S.-S., N.P., A.M., B.P. and A.Š.; resources, B.S.-S. data curation, B.S.-S.; writing—original draft preparation, B.S.-S., N.P., A.M., and A.Š.; writing—review and editing, B.S.-S., A.M. and A.Š.; visualization, B.S.-S.; supervision, B.S.-S.; project administration, B.S.-S.; funding acquisition, A.M. and A.Š. All authors have read and agreed to the published version of the manuscript.

**Funding:** This research received no external funding.

**Data Availability Statement:** Not applicable.

**Conflicts of Interest:** The authors declare no conflict of interest.

#### References

1. Maleki, H.; Durães, L.; Portugal, A. An overview on silica aerogels synthesis and different mechanical reinforcing strategies. *J. Non-Cryst. Solids* **2014**, *385*, 55–74. [[CrossRef](#)]
2. Duan, Y.; Jana, S.C.; Lama, B.; Espe, M.P. Hydrophobic silica aerogels by silylation. *J. Non-Cryst. Solids* **2016**, *437*, 26–33. [[CrossRef](#)]
3. Fedyukhin, A.V.; Strogonov, K.V.; Soloveva, O.V.; Solovev, S.A.; Akhmetova, I.G.; Berardi, U.; Zaitsev, M.D.; Grigorev, D.V. Aerogel Product Applications for High-Temperature Thermal Insulation. *Energies* **2022**, *15*, 7792. [[CrossRef](#)]

4. Miros, A.; Psiuk, B.; Szpikowska-Sroka, B. Aerogel insulation materials for industrial installation: Properties and structure of new factory-made products. *J. Sol-Gel Sci. Technol.* **2017**, *84*, 496–506. [[CrossRef](#)]
5. Wang, J.; Zhang, Y.; Wei, Y.; Zhang, X. Fast and one-pot synthesis of silica aerogels via a quasi-solvent-exchange-free ambient pressure drying process. *Micropor. Mesopor. Mater.* **2015**, *218*, 192–198. [[CrossRef](#)]
6. Pedroso, M.; Gomes, M.d.G.; Silvestre, J.D.; Hawreen, A.; Flores-Colen, I. Thermophysical Parameters and Hygrothermal Simulation of Aerogel-Based Fibre-Enhanced Thermal Insulating Renders Applied on Exterior Walls. *Energies* **2023**, *16*, 3048. [[CrossRef](#)]
7. Hrubesh, L.W.; Poco, J.F. Thin aerogel films for optical, thermal, acoustic and electronic applications. *J. Non-Cryst. Solids* **1995**, *188*, 46–53. [[CrossRef](#)]
8. Liu, H.; Sha, W.; Cooper, A.T.; Fan, M. Preparation and characterization of a novel silica aerogel as adsorbent for toxic organic compounds. *Colloids Surf. A Physicochem. Eng.* **2009**, *347*, 38–44. [[CrossRef](#)]
9. Wang, C.T.; Wu, C.L.; Chen, I.C.; Huang, Y.H. Humidity sensors based on silica nanoparticle aerogel thin films. *Sens. Actuators B Chem.* **2005**, *107*, 402–410. [[CrossRef](#)]
10. Amiri, T.U.; Moghaddas, J.; Khajeh, S.R. Silica aerogel-supported copper catalyst prepared via ambient pressure drying process. *J. Sol-Gel Sci. Technol.* **2016**, *77*, 627–635. [[CrossRef](#)]
11. Guenther, U.; Smirnova, I.; Neubert, R.H.H. Hydrophilic silica aerogels as dermal drug delivery systems—Dithranol as a model drug. *Eur. J. Pharm. Biopharm.* **2008**, *69*, 935–942. [[CrossRef](#)]
12. Bheekhun, N.; Talib, A.R.A.; Hassan, M.R. Aerogels in Aerospace: An Overview. *Adv. Mater. Sci. Eng.* **2013**, *406065*, 18. [[CrossRef](#)]
13. Poelz, G. Preparation of silica aerogel for Cherenkov counters. *Nucl. Instrum. Methods Phys. Res.* **1982**, *195*, 491–503. [[CrossRef](#)]
14. Reim, M.; Körner, W.; Manara, J.; Korder, S.; Arduini-Schuster, M.; Ebert, H.P.; Fricke, J. Silica aerogel granulate material for thermal insulation and daylighting. *Sol. Energy* **2005**, *79*, 131–139. [[CrossRef](#)]
15. Baetens, R.; Jelle, B.P.; Gustavsen, A. Aerogel insulation for building applications: A state-of-the-art review. *Energy Build.* **2011**, *43*, 761–769. [[CrossRef](#)]
16. Smith, D.M.; Maskara, A.; Boes, U. Aerogel-based thermal insulation. *J. Non-Cryst. Solids* **1998**, *225*, 254–259. [[CrossRef](#)]
17. Wang, X.; Ding, Y.; Chen, Z.; Tang, C.; Ren, X.; Hu, H.; Fang, Q. Measurement of the Kinetics and Thermodynamics of the Thermal Degradation for a Flame Retardant Polyurethane-Based Aerogel. *Energies* **2022**, *15*, 6982. [[CrossRef](#)]
18. Kuang-Sheng, L.; Xiao-Feng, Z.; Chia-Hsing, H.; Shin-Ku, L. The Application of Silica-Based Aerogel Board on the Fire Resistance and Thermal Insulation Performance Enhancement of Existing External Wall System Retrofit. *Energies* **2021**, *14*, 4518.
19. Golder, S.; Narayanan, R.; Hossain, M.R.; Rofiqul Islam, M. Experimental and CFD Investigation on the Application for Aerogel Insulation in Buildings. *Energies* **2021**, *14*, 3310. [[CrossRef](#)]
20. Lakatos, Á. Novel Thermal Insulation Materials for Buildings. *Energies* **2022**, *15*, 6713. [[CrossRef](#)]
21. Michael, M.; Favoino, F.; Jin, Q.; Luna-Navarro, A.; Overend, M. A Systematic Review and Classification of Glazing Technologies for Building Façades. *Energies* **2023**, *16*, 5357.
22. Błaszczyszki, T.; Ślosarczyk, A.; Morawski, M. Synthesis of Silica Aerogel by Supercritical Drying Method. *Procedia Eng.* **2013**, *57*, 200–206. [[CrossRef](#)]
23. Shao, Z.; Wu, G.; Cheng, X.; Zhang, Y. Rapid synthesis of amine cross-linked epoxy and methyl co-modified silica aerogels by ambient pressure drying. *J. Non-Cryst. Solids* **2012**, *358*, 2612–2615. [[CrossRef](#)]
24. Shahzamani, M.; Bagheri, R.; Masoomi, M.; Haghgoo, M.; Dourani, A. Effect of drying method on the structure and porous texture of silica-polybutadiene hybrid gels: Supercritical vs. ambient pressure drying. *J. Non-Cryst. Solids* **2017**, *460*, 119–124. [[CrossRef](#)]
25. Perissinotto, A.P.; Awano, C.M.; de Vicente, F.S.; Donatti, D.A.; Mesquita, A.; da Silva, L.F.; Vollet, D.R. Structure and diffuse-boundary in hydrophobic and sodium dodecyl sulfate-modified silica aerogels. *Micropor. Mesopor. Mater.* **2016**, *223*, 196–202. [[CrossRef](#)]
26. Wu, G.; Yu, Y.; Cheng, X.; Zhang, Y. Preparation and Surface modification mechanism of silica aerogels via ambient pressure drying. *Mater Chem. Phys.* **2011**, *129*, 308–314. [[CrossRef](#)]
27. Shi, F.; Wang, L.; Liu, J. Synthesis and characterization of silica aerogels by a novel fast ambient pressure drying process. *Mater. Lett.* **2006**, *60*, 3718–3722. [[CrossRef](#)]
28. Prakash, S.S.; Brinker, C.J.; Hurd, A.J. Silica aerogel films at ambient pressure. *J. Non-Cryst. Solids* **1995**, *190*, 264–275. [[CrossRef](#)]
29. Mazraeh-shahi, Z.T.; Shoushtari, A.M.; Bahramian, A.R.; Abdouss, M. Synthesis, pore structure and properties of polyurethane/silica hybrid aerogels dried at ambient pressure. *J. Ind. Eng. Chem.* **2015**, *21*, 797–804. [[CrossRef](#)]
30. He, S.; Huang, D.; Bi, H.; Li, Z.; Yang, H.; Cheng, X. Synthesis and characterization of silica aerogels dried under ambient pressure bed on water glass. *J. Non-Cryst. Solids* **2015**, *410*, 58–64. [[CrossRef](#)]
31. Ślosarczyk, A.; Strauchmann, W.; Ziolkowski, P.; Jakubowska, P. Synthesis and characterization of carbon fiber/silica aerogel nanocomposites. *J. Non-Cryst. Solids* **2015**, *416*, 1–3. [[CrossRef](#)]
32. García-Torres, B.A.; Aguilar-Elguezabal, A.; Román-Aguirre, M.; Álvarez-Contreras, L. Synthesis of silica aerogels microspheres prepared by ink jet printing and dried at ambient pressure without surface hydrophobization. *Mater. Chem. Phys.* **2016**, *172*, 32–38. [[CrossRef](#)]
33. Li, Z.; Cheng, X.; He, S.; Shi, X.; Yang, H.; Zhang, H. Tailoring thermal properties of ambient pressure dried MTMS/TEOS co-precursor aerogels. *Mater Lett.* **2016**, *171*, 91–94. [[CrossRef](#)]

34. Ślosarczyk, A.; Baretkowski, M.; Niemier, S.; Jakubowska, P. Synthesis and characterization of silica aerogel/carbon microfibers nanocomposites dried in supercritical and ambient pressure conditions. *J. Sol-Gel Sci. Technol.* **2015**, *76*, 227–232. [[CrossRef](#)]
35. Ślosarczyk, A. Synthesis and characterization of silica aerogel-based nanocomposites with carbon fibers and carbon nanotubes in hybrid system. *J. Sol-Gel Sci. Technol.* **2017**, *84*, 16–22. [[CrossRef](#)]
36. Ślosarczyk, A.; Klapiszewski, Ł.; Buchwald, T.; Krawczyk, P.; Kolanowski, Ł.; Lota, G. Carbon Fiber and Nickel Coated Carbon Fiber–Silica Aerogel Nanocomposite as Low Frequency Microwave Absorbing Materials. *Materials* **2020**, *13*, 400. [[CrossRef](#)]
37. Rao, A.V.; Sakhare, H.M.; Tamhankar, A.K.; Shinde, M.L.; Gadave, D.B.; Wagh, P.B. Influence of N,N-dimethylformamide additive on the physical properties of citric acid catalyzed TEOS silica aerogels. *Mater. Chem. Phys.* **1999**, *60*, 268–273.
38. Parvathy Rao, A.; Venkateswara Rao, A. Study the Influence of Drying Control Chemical Additives on the Physical and Optical Properties of Nanocrystalline Cadmium Sulfide–Doped Tetraethylorthosilicate Silica Xerogels. *J. Mat. Syn. Process.* **2002**, *10*, 1.
39. Nah, H.-Y.; Parale, G.; Jung, H.-N.-R.; Lee, K.-Y.; Lim, C.-H.; Ku, Y.; Park, H.-H. Role of oxalic acid in structural formation of sodium silicate-based silica aerogel by ambient pressure drying. *J. Sol-Gel Sci. Technol.* **2018**, *85*, 302–310. [[CrossRef](#)]
40. Ochoa, M.; Lamy-Mendes, A.; Maia, A.; Portugal, A.; Durães, L. Influence of Structure-Directing Additives on the Properties of Poly(methylsilsesquioxane) Aerogel-Like Materials. *Gels* **2019**, *5*, 6. [[CrossRef](#)]
41. Lamy-Mendes, A.; Pontinha, A.D.R.; Alves, P.; Santos, P.; Durães, L. Progress in silica aerogel-containing materials for buildings' thermal insulation. *Constr. Build. Mater.* **2021**, *286*, 122815. [[CrossRef](#)]
42. Ślosarczyk, A. Recent Advances in Research on the Synthetic Fiber Based Silica Aerogel Nanocomposites. *Nanomaterials* **2017**, *7*, 44. [[CrossRef](#)]
43. Buratti, C.; Belloni, E.; Merli, F.; Zinzi, M. Aerogel glazing systems for building applications: A review. *Energy Build.* **2021**, *231*, 110587. [[CrossRef](#)]
44. Adhikary, S.K.; Ashish, D.K.; Rudžionis, Ž. Aerogel based thermal insulating cementitious composites: A review. *Energy Build.* **2021**, *245*, 111058. [[CrossRef](#)]
45. Ślosarczyk, A.; Garbalińska, H.; Strzałkowski, J. Lightweight alkali-activated composites containing sintered fly ash aggregate and various amounts of silica aerogel. *J. Build. Eng.* **2023**, *74*, 106879. [[CrossRef](#)]
46. Ślosarczyk, A.; Vashchuk, A.; Klapiszewski, Ł. Research Development in Silica Aerogel Incorporated Cementitious Composites—A Review. *Polymers* **2022**, *14*, 1456. [[CrossRef](#)] [[PubMed](#)]
47. He, S.; Li, Z.; Shi, X.; Yang, H.; Gong, L.; Cheng, X. Rapid synthesis of sodium silicate based hydrophobic silica aerogel granules with large surface area. *Adv. Powder Technol.* **2015**, *26*, 537–541. [[CrossRef](#)]
48. Liu, M.L.; Yang, D.A.; Qu, Y.F. Effect of different chemical additives and heat-treatment on ambient pressure dried silica aerogels. *J. Exp. Nanosci.* **2010**, *5*, 83–91. [[CrossRef](#)]
49. Chiappim, J.W.; Awano, C.M.; Donatti, D.A.; de Vicente, F.S.; Vollet, D.R. Structure and Hydrophobic Ambient-Pressure-Dried Aerogels Prepared by Sonohydrolysis of Tetraethoxysilane with Additions of N,N-Dimethylformamide. *Langmuir* **2014**, *30*, 1151–1159. [[CrossRef](#)]
50. Tabata, M.; Adachi, I.; Kawai, H.; Sumiyoshi, T.; Yokogawa, H. Hydrophobic silica aerogel production at KEK. *Nucl. Instrum. Methods Phys. Res. A* **2012**, *668*, 64–70. [[CrossRef](#)]
51. Tabata, M.; Kawai, H. Progress in Development of Silica Aerogel for Particle- and Nuclear-Physics Experiments at J-PARC. *JPS Conf. Proc.* **2005**, *8*, 022004.
52. Yu, H.; Liang, X.; Wang, J.; Wang, M.; Yang, S. Preparation and characterization of hydrophobic silica aerogel sphere products by co-precursor method. *Solid State Sci.* **2015**, *48*, 155–162. [[CrossRef](#)]
53. Rao, A.V.; Lathe, S.S.; Nadargi, D.Y.; Hirashima, H.; Ganesan, V. Preparation of MTMS based transparent superhydrophobic silica films by sol-gel method. *J. Colloid Interface Sci.* **2009**, *332*, 484–490.
54. Szpikowska-Sroka, B.; Pawlik, N.; Goryczka, T.; Pisarski, W.A. Influence of silicate sol-gel host matrices and catalyst agents on the luminescent properties of Eu<sup>3+</sup>/Gd<sup>3+</sup> under different excitation wavelength. *RSC Adv.* **2015**, *5*, 98773–98782. [[CrossRef](#)]
55. Matias, T.; Marques, J.; Quina, M.J.; Gando-Ferreira, L.; Valente, A.J.M.; Portugal, A.; Durães, L. Silica-based aerogels as adsorbents for phenol-derivative compounds. *Colloids Surf. A Physicochem. Eng. Asp.* **2015**, *480*, 260–269. [[CrossRef](#)]
56. Smitha, S.; Shajesh, P.; Aravind, P.R.; Kumar, S.R.; Pillai, P.K.; Warriar, K.G.K. Effect of aging time and concentration of aging solution on the porosity characteristics of subcritically dried silica aerogels. *Micropor. Mesopor. Mater.* **2006**, *91*, 286–292. [[CrossRef](#)]
57. Zhou, B.; Shen, J.; Wu, Y.; Wu, G.; Ni, X. Hydrophobic silica aerogels derived from polyethoxydisiloxane and perfluoroalkylsilane. *Mater. Sci. Eng. C* **2007**, *27*, 1291–1294. [[CrossRef](#)]
58. Malik, A.S.; Dabbs, D.M.; Katz, H.E.; Aksay, I.A. Silica Monoliths Templated on L<sub>3</sub> Liquid Crystals. *Langmuir* **2006**, *22*, 325–331. [[CrossRef](#)]
59. Aguiar, H.; Serra, J.; González, P.; León, B. Structural study of sol-gel silicate glasses by IR and Raman spectroscopies. *J. Non-Cryst. Solids* **2009**, *355*, 475–480. [[CrossRef](#)]
60. Riegel, B.; Hartmann, I.; Kiefer, W.; Groß, J.; Fricke, J. Raman spectroscopy on silica aerogels. *J. Non-Cryst. Solids* **1997**, *211*, 294–298. [[CrossRef](#)]
61. Snyder, R.G.; Hsu, S.L.; Krimm, S. Vibrational spectra in the C-H stretching region and the structure of the polymethylene chain. *Spectrochim. Acta A* **1978**, *34*, 395–406. [[CrossRef](#)]
62. Amonkosolpan, J.; Wolverson, D.; Goller, B.; Polisski, S.; Kovalev, D.; Rollings, M.; Grogan, M.D.W.; Birks, T.A. Porous silicon nanocrystals in a silica aerogel matrix. *Nanoscale Res. Lett.* **2012**, *7*, 397–402. [[CrossRef](#)]

63. Bae, S.C.; Lee, H.; Lin, Z.; Granick, S. Chemical Imaging in a Surface Forces Apparatus: Confocal Raman Spectroscopy of Confined Poly(dimethylsiloxane). *Langmuir* **2005**, *21*, 5685–5688. [[CrossRef](#)] [[PubMed](#)]
64. Nazriati, N.; Setyawan, H.; Affandi, S.; Yuwana, M.; Winardi, S. Using bagasse ash as a silica source when preparing silica aerogels via ambient pressure drying. *J. Non-Cryst. Solids* **2014**, *400*, 6–11. [[CrossRef](#)]
65. Casula, M.F.; Corrias, A.; Paschina, G. FeCo-SiO<sub>2</sub> nanocomposite aerogels by high temperature supercritical drying. *J. Mater. Chem.* **2002**, *12*, 1505–1510. [[CrossRef](#)]
66. Kamitsos, E.I.; Patsis, A.P. Infrared-reflectance spectra of heat-treated, sol-gel-derived silica. *Phys. Rev. B* **1993**, *48*, 12499–12505. [[CrossRef](#)]
67. Chen, J.Y.; Pan, F.M.; Chang, L.; Chao, A.T.; Chao, K.J. Thermal stability of trimethylsilylated mesoporous silica thin films as the ultralow—K dielectric for cooper interconnects. *J. Vac. Sci. Technol. B* **2005**, *23*, 2034–2040. [[CrossRef](#)]

**Disclaimer/Publisher’s Note:** The statements, opinions and data contained in all publications are solely those of the individual author(s) and contributor(s) and not of MDPI and/or the editor(s). MDPI and/or the editor(s) disclaim responsibility for any injury to people or property resulting from any ideas, methods, instructions or products referred to in the content.